

The SpaceDrive Project - Progress in the Investigation of the Mach-Effect-Thruster Experiment

IEPC-2019-712

*Presented at the 36th International Electric Propulsion Conference
University of Vienna • Vienna, Austria
September 15-20, 2019*

Maxime Monette¹, Matthias Kößling² and Martin Tajmar³

*Institute of Aerospace Engineering, Technische Universität Dresden, Marschnerstrasse 32, 01307 Dresden,
Germany*

Abstract: An innovative concept for propellantless space propulsion, originally proposed by Woodward using the so-called ‘Mach Effect’ and supported by peer-reviewed, experimental evidence, was investigated at TU Dresden in the framework of the SpaceDrive Project. The Mach-Effect-Thruster is a pre-stressed, multilayer piezoelectric stack driven by a sinusoidal voltage at an optimal frequency producing propellantless thrust, orders of magnitude more efficient than a photon rocket. As a follow-up to the previous test campaign, in which no significant thrust could be systematically detected above the noise range of the torsion balance in vacuum, the tests are repeated on a torsion balance with increased sensitivity. Equipped with two A-20 C-Flex pivot bearings, the background noise measured as a standard deviation of the beam displacement was reduced from 200 nN to around 5 nN. In this recent experimental campaign, Woodward’s original equipment, which includes a Carvin audio amplifier and a 1:4 transformer in the driving electronics, was used. A force signal qualitatively similar to the effect described by Woodward could be observed. The switching on-off transients of 30 nN were, however, were significantly smaller than the force previously claimed at a similar voltage. Furthermore, the force signal was also observed when orienting the MET’s theoretical ‘thrust’ vector parallel to the balance beam which should show zero thrust. In addition to these experiments, the mutual influence of the driving electronics and its piezoelectric load is carefully analyzed in a range of 24 to 48 kHz, the balance is fully characterized with a purely resistive dummy load, and is calibrated along its three principal axes using a voice coil. Finally, this paper presents an investigation of the thermal, vibration and electromagnetic artefacts that can occur in such torsion balance measurements.

Nomenclature

ζ = Damping ratio [dimensionless]

Abbreviations

AWG = American Wire Gauge
BNC = Bayonet Neill-Concelman
DC = Direct Current
DOF = Degree Of Freedom
FE = Finite Element
FFT = Fast Fourier Transform
MET = Mach-Effect-Thruster
PEEK = Polyether-ether-ketone
PZT = Lead-Zirconium-Titanate
SHM = Simple Harmonic Motion

I. Introduction

Current propulsion technologies are primarily limited by Tsiolkovsky’s rocket equation, which entails the use of astronomic quantities of propellant when considering interstellar space travel. Using laser beam propulsion, having a theoretical force of 3.3 nN/W, sending a small payload to the nearest star within a reasonable timeframe would require GW lasers, in addition to other technological limitations¹. The SpaceDrive project aims to

¹ Ph.D. Candidate, Chair of Space Systems, maxime.monette@tu-dresden.de.

² Ph.D. Candidate, Chair of Space Systems, matthias.koessling@tu-dresden.de.

³ Professor, Department Head, Chair of Space Systems, martin.tajmar@tu-dresden.de

investigate experimental propulsion systems that promise better than photon-propulsion, and propellantless propulsion methods that would revolutionize interstellar space travel. The two main concepts under investigation so far are the Mach-Effect-Thruster and the EmDrive in addition to a variety of other novel concepts².

A torsion balance is developed to investigate controversial claims of propellantless thrust in the literature that involve very small forces. In the EmDrive experiments, the observed forces are smaller than $90 \mu\text{N}^3$, whereas in the Mach-Effect-Thruster (MET) experiments, the forces can be under $1 \mu\text{N}^4$. Validating forces would lead to the possibility of major scaling up. Measuring forces at a smaller scale, however, first requires a good characterization of the balance and the surroundings in order to avoid the pollution of force measurements. This paper presents measurements of the forces involved when powering the MET on a balance with a resolution as low as 2 nN.

The MET is a device invented by Woodward that aims to produce unidirectional thrust without the use of propellant and of greater efficiency than the photon rocket. According to Woodward, unidirectional thrust can be induced when driving a pre-stressed, multi-layered, piezoelectric stack actuator sandwiched between different tail and head masses by the generation of mass fluctuations due to Mach effects⁵. The driving frequency should be close to mechanical resonance and present high non-linearity. According to Woodward, the phenomenon can be explained. Claims of thrust on a torsion balance when commanding a sinusoidal signal with voltage amplitude between 200-250 V are between 1 and 5 μN with even larger on-off transients⁶. Buldrini replicated the experiment and reported a smaller measured force of 0.2 μN at a lower voltage amplitude of 100 V⁷. In our previous test campaign, different device models, driving frequencies and voltages, as well as different driving conditions were tested but no signal above the balance noise were observed⁸. Significant was the fact that the previous tests used a different amplifier than Woodward's, and that the driving conditions were locked on the mechanical resonance of the device for a maximal power transfer, by an automatically implemented frequency tracker. Adding a step-up transformer to the electronics setup seems to have had no impact on the results.

Thus, the force measurements were repeated this time using the same electronics and device used by Woodward and with a torsion balance with increased sensitivity. Section II describes the balance and calibration experiments, section III describes the MET experiment and results.

II. Thrust Balance

The design of the new torsion balance follows the design described in reference 8. Hence, only the few key points allowing the achievement of a better resolution for devices with smaller masses will be mentioned. All experiments were performed in a vacuum chamber at an ambient pressure of $8 \cdot 10^{-2}$ mbar to remove the influence of buoyancy and convective effects on the force measurements.

A. Features

The balance (Figure 1a, b) has a beam length of 700 mm. The displacement measurement, the calibration coil and the device-under-test are located 340 mm away from the center of the beam. The displacement of the balance beam is measured using an attocube IDS3010 with a M12/C1.6 sensor head. The main difference between the previous described balance and the new balance is the pivot. The new balance uses two A-20 bearings, with a torsional spring rate of $k = 0.20 \text{ mN}\cdot\text{m}^\circ$ that is much lower than the E-20 bearings used in the previous version. The new pivots also define a new maximal weight to be placed on the balance of 5.7 kg, compared to a previous 35.0 kg, and a maximal allowable weight disparity between the opposite ends of the balance of 0.25 kg, compared to a previous 3.00 kg. The smaller maximum weight and a similar beam length result in a lower moment of inertia of $0.17 \text{ kg}\cdot\text{m}^2$, compared to a previous $1.69 \text{ kg}\cdot\text{m}^2$. The power for electronics and experiments is transmitted via four liquid contacts (Figure 2). The AWG24 BNC cables are each connected through RG174 BNC connectors.

To calibrate the balance, a LVCM-010-013-01 voice coil from Moticont is used (Figure 3, left). On one hand, the voice coil's relatively large stroke of 6 mm renders the need for an alignment mechanism with motor obsolete. On the other hand, it introduces a non-linearity in the dependence of the exerted force on the distance between the solenoid and the permanent magnet. A detailed analysis of the calibration is presented in section 0. The damping mechanism (Figure 3, right) is similar to the older balance's. It consists of two N35 neodymium magnets ($\varnothing 30 \times 3$ mm, 1.2 T) placed on either inner sides of a U-shaped steel bracket (1.0503) mounted on the beam. A fixed, 2 mm-thick copper plate is mounted on a slider to adjust the level of damping. Serial communication between the data interface LabJack T4 and other electronic components is performed via two infrared modules (IrDA-to-PC, Mikroelektronika).

B. Voice Coil Calibration

The non-linear behavior of the voice coil was carefully investigated over a wide coil-magnet distance range and for several supplied currents. This specific experiment was not performed in vacuum. The exerted force was measured using a Sartorius AX224 balance, having a resolution of 0.1 mg, the supplied current was measured using a Keithley 2450 current source, and the distance between the coil and magnet was measured using the

attocube IDS3010 fitted with a M12/C1.6 sensor head. A 3-axis Owis translation stage was used to move the solenoid.

The setup (Figure 4) consists of an aluminum profile with one side connected to a pivot and the other resting on the translation stage. The solenoid is mounted 340 mm away from the pivot to recreate the same deflection path that would be seen on the torsion balance. A mirror is placed at the same level as the solenoid, to measure the displacement between the coil and magnet. The magnet is placed on top of two, 6 mm PEEK plates to minimize the electromagnetic interaction of the solenoid on the balance. The minimum distance between the magnet and the solenoid was discovered by lowering the aluminum profile until the balance showed a force above its resolution.

The test was done by applying three different currents to the coil, each test was repeated three times. The tested currents were 200, 600 and 1000 μA . After a series of test at a specific height, the translation stage increased the solenoid-magnet distance.

Figure 5a shows the result for a commanded current of 1000 μA including a polynomial fit with order 3. On the left side, the calibration constant (force over current) is shown.

Figure 5b shows the calibration constant for all three currents. In a solenoid-magnet distance range of 1 to 3 mm, the maximum difference between the factors for different currents was 0.9%. The non-linearity of the voice coil with respect to the solenoid-magnet distance resulted in a 6.2 % discrepancy. Thus, before launching a test on the torsion balance, the voice coil is aligned to have a distance between magnet and solenoid of 2 mm, which corresponds to a voice coil calibration factor of 0.339 $\mu\text{N}/\mu\text{A}$. Although, this factor differs by 14.5 % from the factor of 0.29 $\mu\text{N}/\mu\text{A}$ given in Moticont's datasheet, the manufacturer's calibration is specified for a much greater current of 1 A. Our test was repeated with a second voice coil and the calibration results show great consistency.

Considering little variation over the displacements involved in the tests, as well as good monitoring of the beam position, this calibration factor is used by default for all following calibrations.

C. Balance Calibration

The calibration of the balance is done once before and once after each test. It results in a factor that converts beam displacement to force. The voice coil is used to apply a known force to the balance and the displacement is read with the laser interferometer. The standard calibration profile consists in zero applied current for the first 40 s, then current is applied for 60 s, and again zero applied current for 40 s before the next calibration. The balance needs approximately 15 s to reach steady state, and so the average position of the remaining 45 s is used to calculate the calibration constant. Figure 6 shows the result of a fine calibration which specifically consists of 81 experimental points: 39 profiles were distributed between 10.0 and 340.0 μN , and 42 were distributed between 0.1 μN and 10.0 μN . The calibration was performed with positive (pushing) as well as negative (pulling) forces to verify that the balance responds in both directions the same way. This calibration shows a linear behavior of the balance with a calibration factor of 0.278 $\mu\text{N}/\mu\text{m}$ and a linear correlation of 0.998. The regular calibrations performed before and after each tests usually only consist of 13 different points between -6 and 6 μN , and result in calibration factors that vary between 0.270 and 0.290 $\mu\text{N}/\mu\text{m}$ for the MET setup. The calibration factor may go up to 0.400 $\mu\text{N}/\mu\text{m}$ for a different setup, but the linear correlation stays extremely high with a minimum of 0.984.

D. Reaction Time and Damping

Although the low torsional spring stiffness improves the force measuring accuracy, it is responsible for the relatively large oscillation period and reaction time of the balance. Figure 7 shows the response of the balance to a 30 s calibration pulse of 5 μN , compared to a 1D SHM simulation using empirical parameters. Steady-state is reached after 16 s, while the reaction time necessary to reach 90% of the steady-state value, is 7 s.

The damping of a torsion balance is normally calculated using the logarithmic decrement⁹. In this case this is not feasible, because there is no clear second oscillation visible. A numerical analysis was used by comparing the result of the simulation with different calibration pulses. The damping in the simulation was varied until the experimental and simulated curves matched each other. The result of this analysis is a damping factor of 0.85, which is close to the recommended range for torsion balances¹⁰.

E. Magnetic Shielding and Noise

The balance beam, the experiment and electronics boxes are shielded with 0.5 mm-thick, high permeability, mu-metal plates to reduce the interaction between the power cables and Earth's magnetic field. In order to test the efficiency of the electromagnetic shielding, the deflection of the balance beam was examined when commanding a 0.8 A, DC current through an 18 Ω resistor placed in the experiment box. The current flowed through the liquid contacts, and through a BNC cable to reach the resistor. The resistor setup with its thermocouple in the opened experiment box can be seen in Figure 8. Figure 9 shows the measured force after removal of the linear thermal drift existing before the current is supplied, the current and the temperature of the resistor respectively. The measured force and temperature start to increase after the power is applied, resulting in a maximal artefact of 30 nN. It can be assumed that this force is caused by the temperature change of the resistor. This assumption is

reinforced by the fact that the force does not go back immediately to its original position after the current is cut off, and instead returns slowly with the slow cooling of the resistor. The absence of on-off transients in the beam displacement indicates good electromagnetic shielding.

The noise during our measurements can be measured from the standard deviation of the beam deflection before any signal is commanded. It is typically 2.1 nN, with an upper limit of 5.2 nN and a lower limit of -4.6 nN. This very low noise is also a result of signal averaging performed by the attocube software at a sampling frequency of 10 Hz.

F. Consideration of Off-axis Forces

In the event that the balance beam is not perfectly level, forces in the vertical and longitudinal axes will also bring about a deflection in the position read by the interferometer, which can be mistaken for a force in the perpendicular direction. Two tests were performed in an attempt to quantify the magnitude of this error for an unloaded balance beam.

Therefore, other than the voice coil used to calibrate the balance in the perpendicular direction, a second voice coil was mounted on the beam to apply forces along the longitudinal and vertical axes alternatively. Figure 10 shows the setup for the test of vertical forces. The applied force for both tests was set to 100 μ N and the results are shown in Figure 11 and Figure 12. It can be seen, indeed, that the balance responds to these forces to a very limited extent. The response to the vertical force is approximately 250 times smaller than the applied force and the response for the longitudinal force is approximately 500 smaller. These results are explained by the minute discrepancy in the beam orientation, which does not change significantly when a device is mounted on the balance beam.

III. Mach-Effect-Thruster Experiments

A. Experimental Setup

The device to be tested on the torsion balance described was provided by Woodward himself. The device (NS5) consists in a stack formed of eight, 2 mm-thick disks of SM111 (PZT4) material with 19 mm diameter, supplied by Steiner & Martins (Figure 13). The piezo-disks are glued together in a stack with an epoxy using EPON Resin 815C. Between each disk is a very thin copper electrode (<100 μ m-thickness) of similar diameter with an elongated tab. In order to establish a parallel electric connection, each disk is connected to the adjacent disk with matching polarity, and the corresponding poles are joined at the electrode tab using solder and sections of 28 AWG electrical wire. Towards the outer end of the stack is a pair of 0.3 mm-thin disks, squeezed between disk pairs of the same diameter and piezomaterial. The negative pole of these thin disks is connected to the negative pole of the stack and to the conductive base of the device. Their positive pole is however separated from the rest, and is to be read as an accelerometer signal to show the relative vibration amplitudes present in the stack. The whole stack is pre-stressed between a brass mass – 19 mm long, 28.5 mm in diameter – and an aluminum mass – 4.7 mm long, 28.5 mm in diameter – by the means of six 39.5 mm long, 2-56 UNC screws. On the other side of the brass mass are six 15 mm long, 4-40 UNC screws that compress 1 mm-thick synthetic rubber material between the brass mass and an off-the-shelf 3 mm-thick aluminum L-bracket. The screws on either side of the stack are tightened with a torque of 0.45 N·m using an appropriate torque wrench.

In Woodward's original setup, the L-bracket is connected to the mu-metal experiment box acting as a Faraday cage by a 15 mm long, 8-32 UNC screw and a piece of Plexiglas as washer. The experiment box is then connected via a so-called "vibration isolating yoke" that aims to attenuate vibration transmission to the balance beam. Our setup consists in a connection of the device's L-bracket to a piece of high-density polymer (PEEK) in the mu-metal experiment box. A 250 g rectangular block of copper is used as a heat sink. The latter is connected without provision for vibration attenuation to the balance beam. The box can also be rotated by an electric motor through a gear connection. In Figure 14, the device is shown in the 180° orientation, brass mass on the right, which should show a steady thrust towards the right according to Woodward's observation. This hypothesis leads to a positive beam deflection for this 180° configuration. The 0° orientation is for a device that is flipped and the brass mass is on the right. The 90° orientation has the device's longitudinal axis aligned with the balance beam, the brass mass being away from the balance pivot.

Two different sets of electronics to drive the MET were used for comparison. Fullerton electronics consist in the same equipment used by Woodward: a Carvin DCM1000 audio-amplifier and a self-wound 1:4 transformer, the primary side having an inductivity of 265 μ H. Dresden electronics consist in two power amplifier chips (PA04 APEX), supplied by two EA-PS5000 power supplies, that are connected in bridge mode to supply a fixed 180 V to the device. Both sets of electronics use a Picoscope 5442B digital oscilloscope as a frequency generator, and to read amplifier output voltage, current and accelerometer voltage signals (Figure 15). Voltage signals are picked up by differential probes with dividing factors of 100 and 20 respectively (Picoscope, TA041). Current is measured using a current transducer from LEM (LTS 6-NP).

First, the deflection of the beam, as observed by our laser interferometer with a sampling frequency of 10 Hz, was monitored during a frequency sweep of the device. The commanded voltage is fixed and the sweep starts at 48 kHz and is ramped down in frequency with discrete steps of 10 Hz every 10 ms until 24 kHz. The objective of this experiment was to obtain the frequencies at which the beam deflection is maximum.

The second set of experiments consists in test runs of 16 s long pulses of sinusoidal driving signals at a fixed command voltage and fixed frequency, the values of which were specified by Woodward's experiments. During the test, the beam deflection is again monitored with a sampling of 10 Hz in order to limit the size of the data file. An hour was allowed between the test runs in order for the device to cool down.

Lastly, beam deflection was also monitored with greater sampling frequency (25 MHz) during frequency sweeps on the torsion balance to investigate the vibration of the balance beam above 10 Hz.

B. Electromechanical Characterization

Frequency spectra of the device are obtained by commanding a sinusoidal signal, sweeping the frequency between 48 and 24 kHz, and recording voltage and current. With the device disconnected from amplifier electronics, the unloaded spectrum of NS5 is obtained, showing maxima in the accelerometer signals. These represent vibrational amplitude peaks that occur at the stack's resonances (Figure 16). This unloaded spectrum represents a way of characterizing the MET, to identify resonances and detect material ageing, independent of the complex characteristics of the power electronics. Using the stack geometry, a straightforward single DOF calculation shows the main longitudinal resonance of the stack to be around 34 kHz. Other accelerometer signal maxima in the frequency spectrum could be associated with the resonance of the screws¹¹. A more detailed FE analysis is outside of the scope of this paper and will be covered in subsequent papers.

In the first loaded frequency spectrum, the device is connected to Fullerton electronics. For a fixed commanded voltage, the amplifier output voltage and current, as well as the accelerometer signal of the device are shown to vary greatly with frequency (Figure 17). An FFT analysis is used to extract the amplitude of the first harmonic signals. The graph shows the introduction of fluctuations in the output signals, significant non-linearity, and a shift in resonance frequencies compared to the unloaded spectrum. Not shown in the diagram, however, is the presence of higher harmonic signals that are superposed to the output signals oscillating at the commanded frequency. The spectrum shows the non-linearity introduced by the Carvin audio amplifier in the frequency range of interest, which is not designed to drive a load with highly varying impedance and above 20 kHz.

In the second loaded frequency spectrum, the device is connected to Dresden electronics, which include dedicated power amplifiers. Results of the FFT show less variation in the output signals for a fixed commanded voltage over the whole frequency sweep (Figure 18). At a fixed output voltage, the current and accelerometer signals show clear peaks at the resonances of the device. The superposition of second harmonic signals to the commanded signals is significant at the resonances, as has been observed for Langevin transducers before¹². Interestingly, the resonances and second harmonic signal peaks observed occur at different frequencies when comparing how NS5 is driven using either Fullerton or Dresden electronics. The latter spectrum shows resonances closer to the resonances of the device as seen in the unloaded spectrum.

C. Results & Discussion

Figure 19a shows a single sweep using Fullerton electronics with 0° orientation resulting in a negative force of 1 μN where the commanded frequency is around 36 kHz. Recoil of the torsion beam in the other direction, however, results in a permanent, positive offset in the beam position of around 2 μN once the signal is cut off. This behavior could not be systematically repeated. Although no offset can be observed after performing a sweep with Dresden electronics (Figure 19b), a force of -90 nN can be noted when 34 kHz are commanded, around the mechanical resonance of the device. The sweep with Fullerton electronics and the MET oriented at 90° shows an effect with similar magnitude and permanent offset as in the 0° test (Figure 19c). This result cannot be explained by a thrust produced by the device, with its theoretical thrust vector oriented parallel to the balance beam. The offset hints at a shift in the center of mass of the balance beam, due to a shift in position of one of the experiment components and hints at vibration artefacts. The onset of the forces as well as the behavior observed in the sweeps were, again, not exactly repeatable.

When driving the device with a fixed frequency, force traces similar to the ones observed by Woodward are detected: switching transients reversing with the device orientation. However, the forces observed are significantly smaller. The plots in all orientations represent an average of 4-5 profiles with linear balance drift removal. With Fullerton electronics, on-off transient pulses of 20 nN amplitude are present and reverse with the orientation of the device (Figure 20a and Figure 20b). Rather than a significant, steady-state force during powering of the device, swing back behavior in response to the switching transients is observed. The same phenomenon, with switching transients of 60 nN are observed when the device is placed in the 90° orientation, although zero thrust is expected (Figure 20c).

Then, different test conditions are compared with the MET maintained at a 180° orientation. Without the copper block, the device is directly fixed to the PEEK part and the electromechanical spectrum of the system is shifted. As a result, the current and voltage over the device at the same frequency are different and the beam deflection is slightly affected when comparing Figure 21a to Figure 20b. With the vibration isolation yoke provided by Woodward, the characteristics of the device are also expected to be different, which is shown in the voltage and current behavior, but a similar beam deflection to the previous is observed (Figure 21b). At a commanded frequency of 30 kHz, although the current and voltage are quite different than for 36 kHz commanded, the force signal is very similar (Figure 21c). With Dresden electronics, once again although the output voltage and current are different, the force signal is similar to the reference tests (Figure 21d). Another important observation is that the large forces observed in the sweeps were not obtained in individual fixed frequency profiles. Furthermore, the commanded frequency or mounting conditions did not have a significant influence on the magnitude of the switching transients observed.

It was quite difficult to maintain all parameters constant when solely varying the device orientation. For instance, it was observed that the bracket-side screws got looser following experiments and had to be retightened to the specified torque. Furthermore, as the MET got warmer, its electromechanical spectrum also changed which made consecutive tests prone to error and lack repeatability. These differences could account for the slightly different voltages and currents, as well as the different vibration amplitudes observed between test runs with otherwise similar parameters.

Subsequently, the displacement of the balance beam was analyzed using greater sampling frequency during the MET frequency sweeps. First, careful observation led to the identification of ambient noise with maximum 250 nm in amplitude at 20 Hz, which is otherwise filtered out by the attocube software. The origin of this noise is still unknown. Secondly, it was observed that random fluctuations in the output voltage of the Carvin amplifier sometimes led to the appearance of low amplitude mechanical vibration of the beam at 500 Hz. The same characteristic vibration was observed when sweeping the commanded frequency of the MET with Dresden electronics around the resonance frequencies of the device. Figure 22 shows the evolution of the beam vibration for a fixed output voltage during a frequency sweep of around 32.5 kHz. In the time window considered, the commanded frequency only varied by 60 Hz. Lastly, the maximum mechanical vibration amplitudes were consistently observed around the resonance frequencies, where a surge in the second harmonic signals is also seen, in either electronics setups. This phenomenon demands further investigation.

Given the careful precautions to eliminate the electromagnetic interactions between the device, cables on the balance, and the support structure, it is safe to assume that the forces observed are not electromagnetic. The similarity of the beam deflection amplitude when the device is oriented perpendicularly to the beam, and when it is parallel to the beam, however, does not support the hypothesis of uniaxial thrust generation. This result suggests the presence of moments that twist the balance arm or a shift in the center of mass of the balance beam during the experiment. Furthermore, the observation of vibration transmission to the balance beam, also observed in the presence of a vibration isolation yoke and in all device orientations, seems to indicate the presence of a vibrational artefact.

IV. Conclusion

This paper showcases the results of Mach-Effect-Thruster experiments using Woodward's original equipment on a new torsion balance. The thrust balance was characterized and shows high linearity in the calibration as well as a very low, average signal noise of 2 nN. The balance's mu-metal shielding seems to exclude reaction to electromagnetic effects generated inside the balance beam, or experiment box, as demonstrated by the null result in a dummy test with a DC current of 0.8 A. Balance calibration using voice coils along the beam's three major axes show the expected absence of significant balance response for forces along the longitudinal and vertical axes.

MET experiments using fixed frequency and frequency sweeps were conducted in vacuum with a device from Woodward (NS5), the original Carvin audio amplifier and a transformer. Results qualitatively showed the expected signal with switching on-off transients and dependence on orientation. The experiments also showed, however, forces of similar amplitude, when the device was placed parallel to the torsion beam which is not consistent with the hypothesis of uniaxial thrust generation pointing instead towards a vibration artefact. Furthermore, changing the electronics, mounting or driving frequency did not increase the force past 100 nN, which is an order of magnitude below claims by Woodward. Sweeping frequency tests sometimes showed jumps of up to 3 μN, but the balance beam did not go back to its original position and the same behavior was observed for a device oriented parallel to the balance beam. Study of beam vibrations also shows transient vibration of a few hundred nN, stemming from the non-linear behavior of the electromechanical system close to its resonances.

In order to definitely rule out the possibility of vibration transmission to cause false positive force signals, the experiments will be replicated on other types of balances. Under development at TU Dresden are two additional types of balance: the double-pendulum balance, which should be less sensitive to shifts in the center of mass of the experiment, and a rotating balance with levitating superconductor as a pivot aiming to show production of

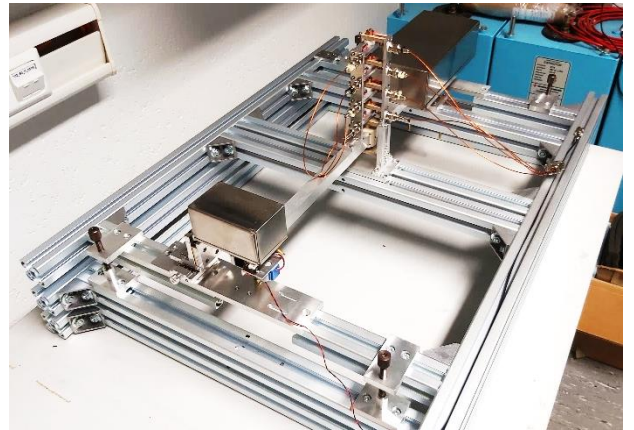
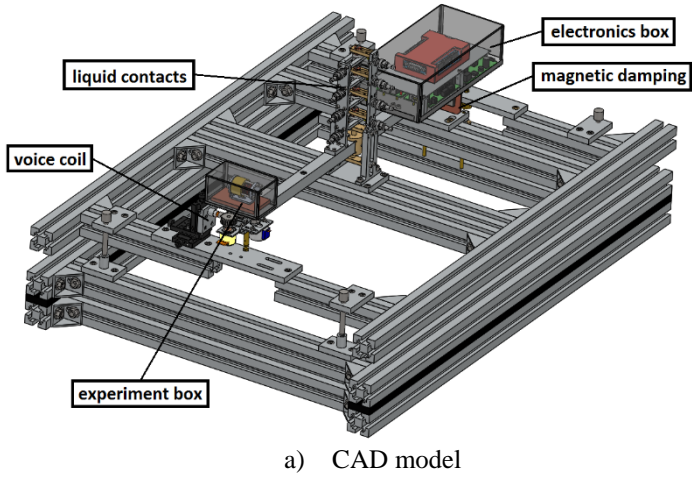
thrust from devices over a 360° rotation of the balance arm¹³. These additional experiments will then hopefully settle the case for the Mach-Effect-Thruster.

Acknowledgements

We gratefully acknowledge the support for SpaceDrive by the German National Space Agency DLR (Deutsches Zentrum fuer Luft- und Raumfahrttechnik) by funding from the Federal Ministry of Economic Affairs and Energy (BMWi) by approval from German Parliament (50RS1704). We would also like to acknowledge the support from J. Heisig, J. Woodward, H. Fearn and J. Rodal for their contributions to the ongoing experiments and discussions.

References

- [1] Frisbee, R. H., Edited by Millis, M., *Frontiers of Propulsion Science*, 2009, pp. 31-106. doi:10.2514/4.479953
- [2] Tajmar, M., Kößling, M., Weikert, M., and Monette, M., “The SpaceDrive Project - Developing Revolutionary Propulsion at TU Dresden,” *Acta Astronautica*, vol. 153, 2018, pp. 1-5. doi: 10.1016/j.actaastro.2018.10.028
- [3] White, H., Lawrence, J., March, P., Vera, J., Sylvester, P., and Bailey, P., “Measurement of Impulsive Thrust from a Closed Radio-Frequency Cavity in Vacuum,” *Journal of Propulsion and Power*, vol. 33, 2016, pp. 1–12. doi:10.2514/1.B36120
- [4] Fearn, H., and Woodward, J. F., “New Experimental Results for Mach Effect Gravitation Assist (MEGA) Drives,” *AIAA Propulsion and Energy Forum NNF*, Indianapolis: 2019. doi:10.2514/6.2019-4285. doi:10.2514/6.2019-4285
- [5] Woodward, J. F., *Making Starships and Stargates*, Springer New York, 2013.
- [6] Fearn, H., and Woodward, J., “Recent Results of an Investigation of Mach Effect Thrusters,” *AIAA Journal*, 2012. doi:10.2514/6.2012-3861
- [7] Buldrini, N., “Verification of the thrust signature of a Mach effect device, “ in: H. Fearn, L. Williams (Eds.), *Proceedings of the Estes Park Advanced Propulsion Workshop*, Space Studies Institute Press, Mojave, CA, 2017, pp. 83–88.
- [8] Kößling, M., Monette, M., Weikert, M., and Tajmar, M., “The SpaceDrive Project - Thrust Balance Development and New Measurements of the Mach-Effect and EMDrive Thrusters,” *Acta Astronautica*, vol. 161, 2019, pp. 139–152. doi: 10.1016/j.actaastro.2019.05.020
- [9] Soni, J., and Roy, S., “Design and Characterization of a Nano-Newton Resolution Thrust Stand,” *Review of Scientific Instruments*, 2013. doi:10.1063/1.4819252
- [10] Polk, J. E., Pancotti, A., Haag, T., King, S., Walker, M., Blakely, J., and Ziemer, J., “Recommended Practice for Thrust Measurement in Electric Propulsion Testing,” *Journal of Propulsion and Power*, vol. 33, 2017doi:10.2514/1.B35564
- [11] DeAngelis, D. A., Schulze, G. W., and Wong, K. S., “Optimizing Piezoelectric Stack Preload Bolts in Ultrasonic Transducers,” *43rd Annual Symposium of the Ultrasonic Industry Association*, 2015. doi:10.1016/j.phpro.2015.03.003, pp. 11–20. doi:10.1016/j.phpro.2015.03.003
- [12] Guyomar, D., Aurelle, N., Eyraud, L., Guyomar, D., Aurelle, N., Piezoelectric, L. E., Nonlinear, C., Application, B., Journal, T., Iii, D. P., Sciences, E. D. P., and Lyon, I., “Piezoelectric Ceramics Nonlinear Behavior. Application to Langevin Transducer,” *Journal de Physique III*, vol. 7, 1997, pp. 1197-1208, doi: 10.1051/jp3:1997183
- [13] Neunzig, O., and Tajmar, M., “Development of a Superconducting Levitation Thrust Balance for Propellantless Propulsion,” *69th International Astronautical Congress*, Bremen: 2018, IAC-18,E2,2,11,x48639.



b) Completed balance

Figure 1: Balance v6

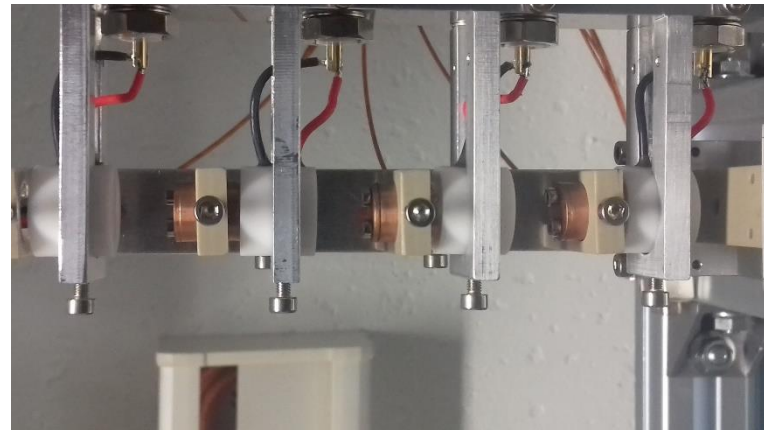


Figure 2: Liquid contacts (left), mounted on the balance (right)

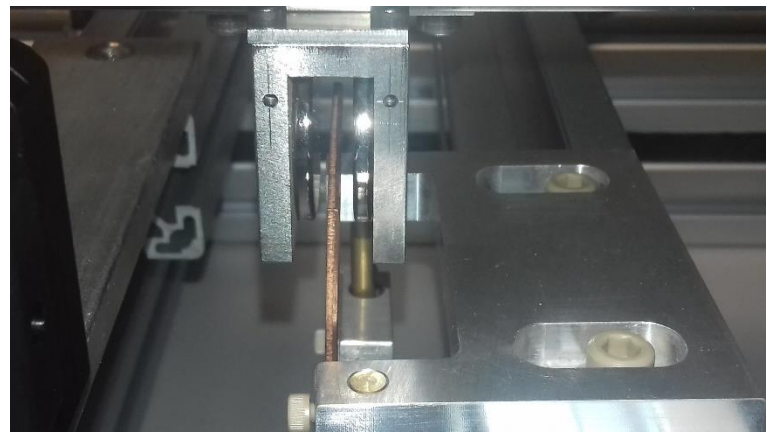
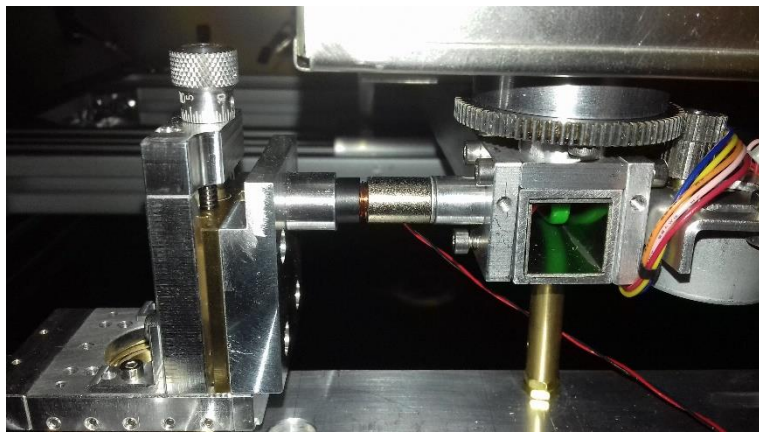


Figure 3: Close-up of the voice coil (left), of the damping (right)

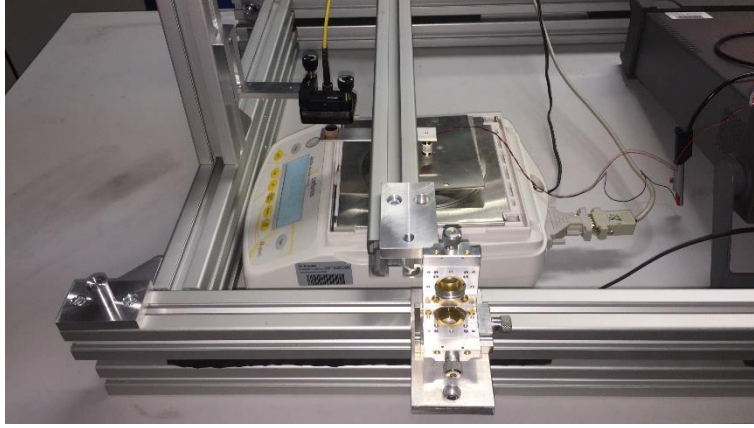
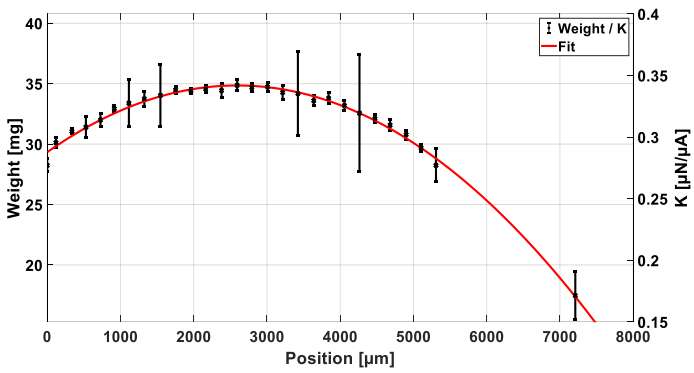
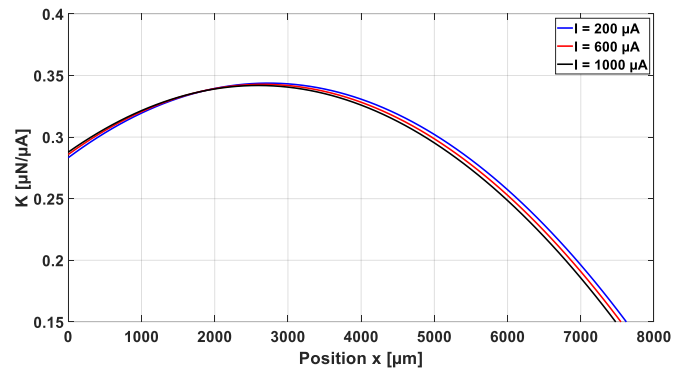


Figure 4: Voice coil Sartorius calibration setup



a) Calibration data for 1000 μA , with standard deviation



b) Calibration fits for 200, 600 and 1000 μA

Figure 5: Voice coil calibration results

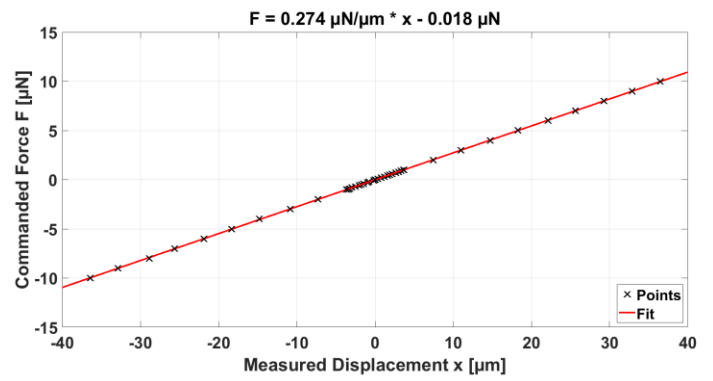
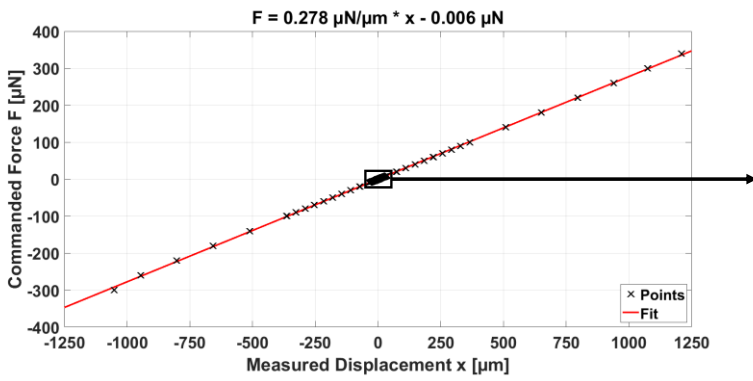


Figure 6: Balance calibration with voice coil

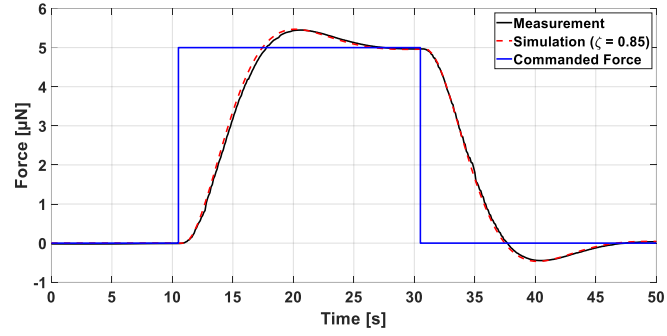


Figure 7: Response time and damping comparison (experiment vs simulation)

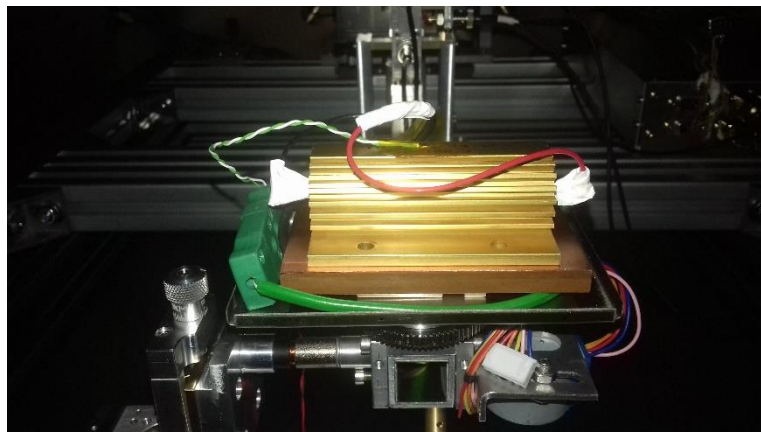


Figure 8: 18 Ω resistor setup (open experiment box)

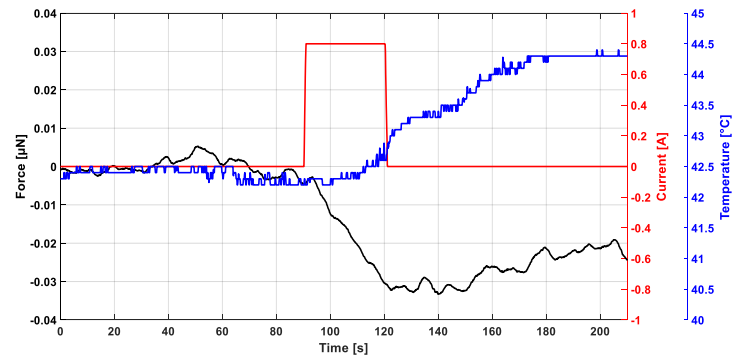


Figure 9: Resistor test, balance drift removed

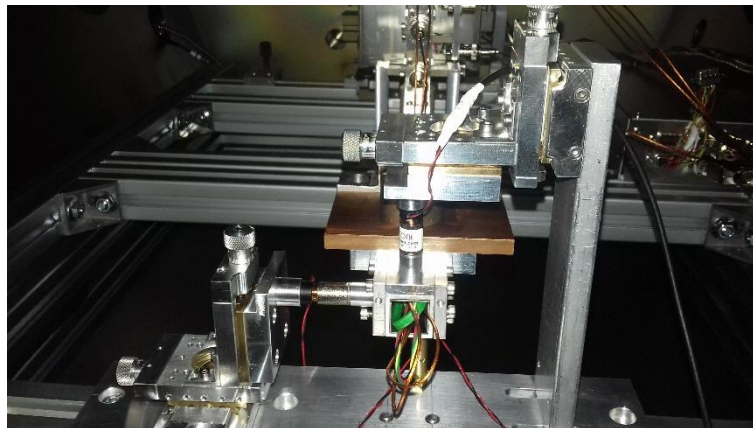


Figure 10: Vertical voice coil test setup

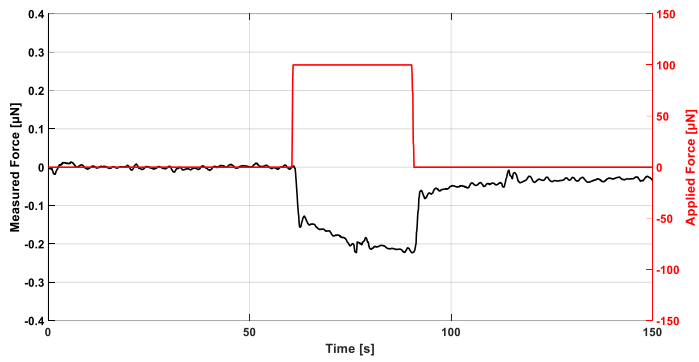


Figure 11: Longitudinal axis voice coil test result

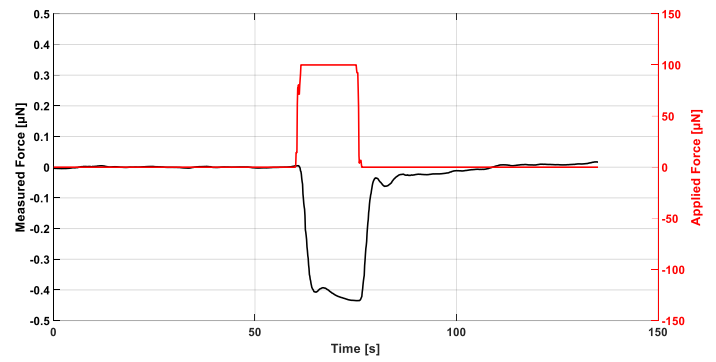


Figure 12: Vertical axis voice coil test result

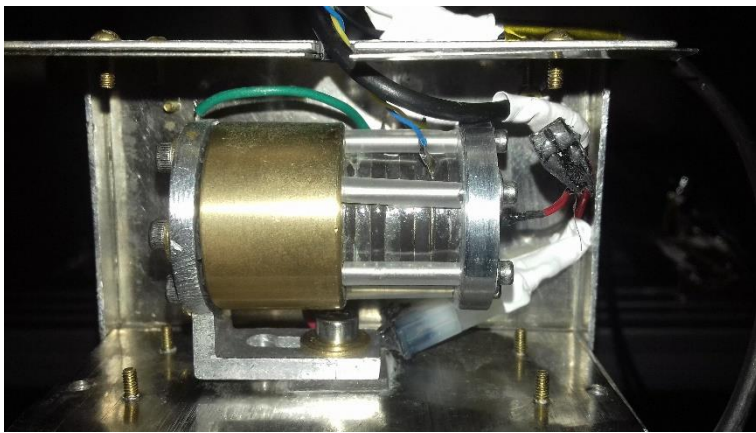


Figure 13: NS5

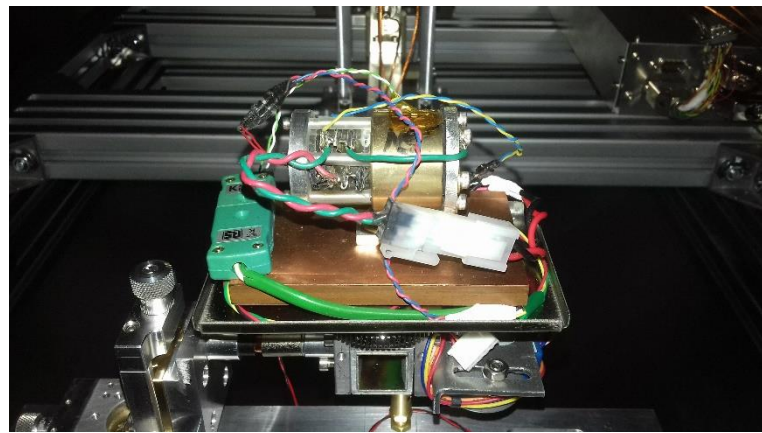


Figure 14: NS5 on with copper block (180°)

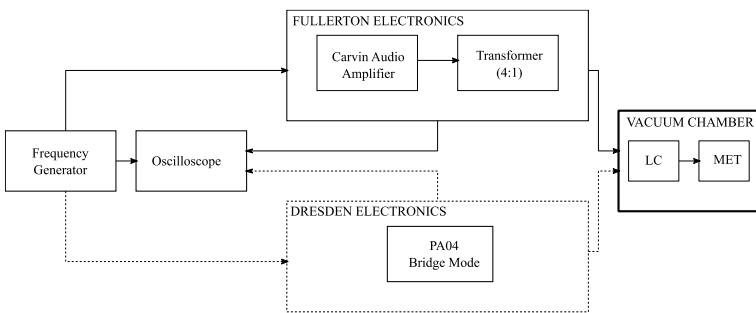


Figure 15: MET experiment setup

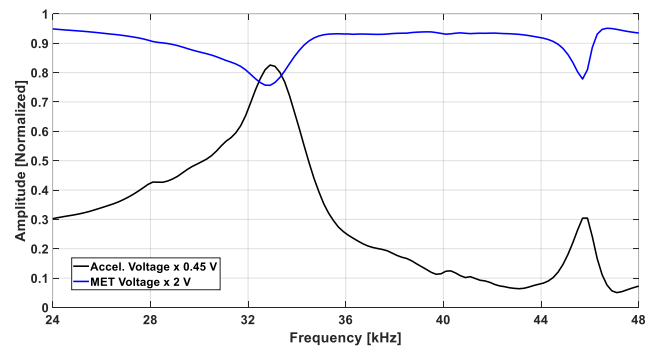


Figure 16: Unloaded spectrum NS5 (2V)

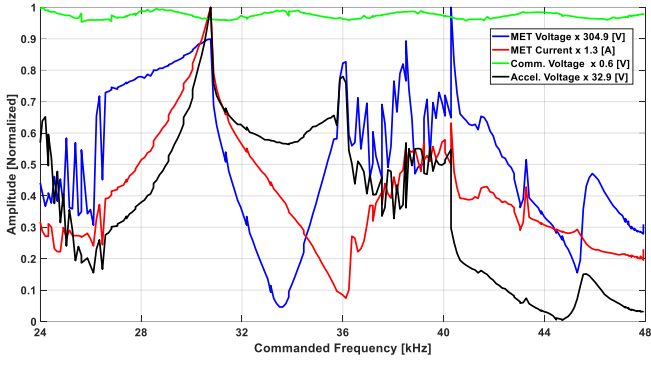


Figure 17: Spectrum of NS5 with Fullerton electronics
First harmonic components

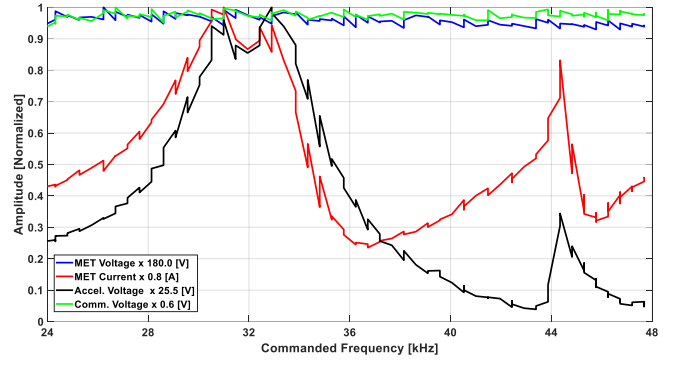
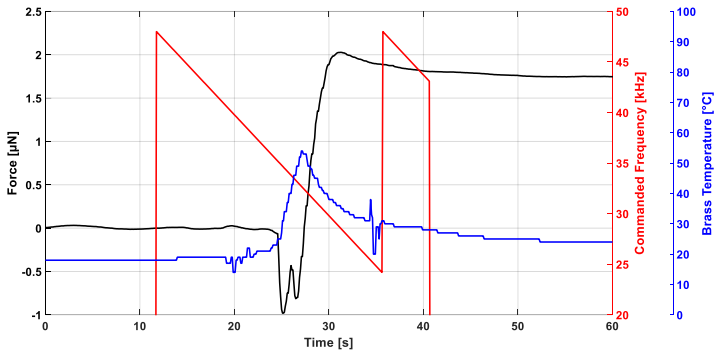
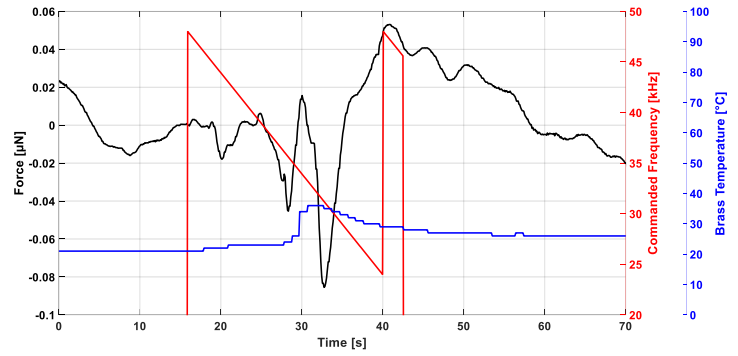


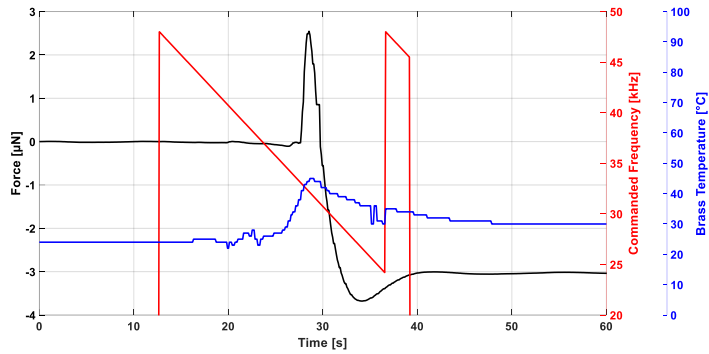
Figure 18: Spectrum of NS5 with Dresden electronics
First harmonic component



a) Fullerton Electronics, 0° orientation, 19-07-30 Sweep8



b) Dresden Electronics, 0° orientation, 19-04-26 Sweep1



c) Fullerton electronics, -90° orientation, 19-07-31 Sweep2

Figure 19: Frequency sweeps of NS5 with temperature and beam deflection

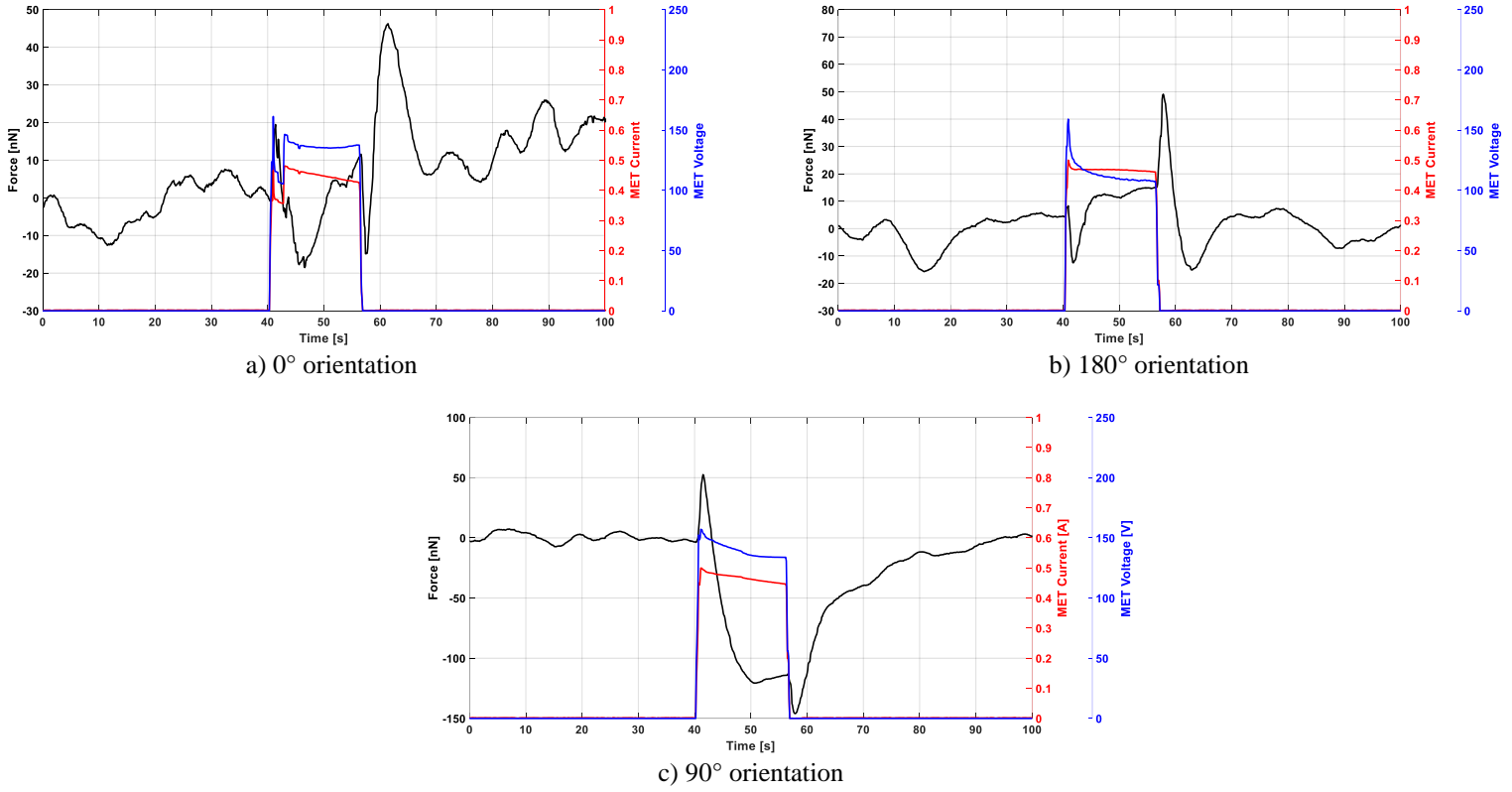
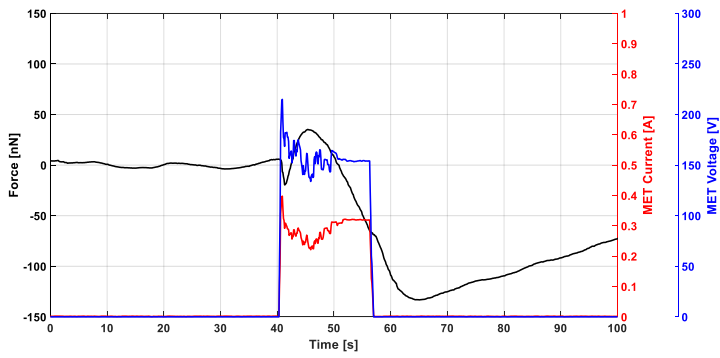
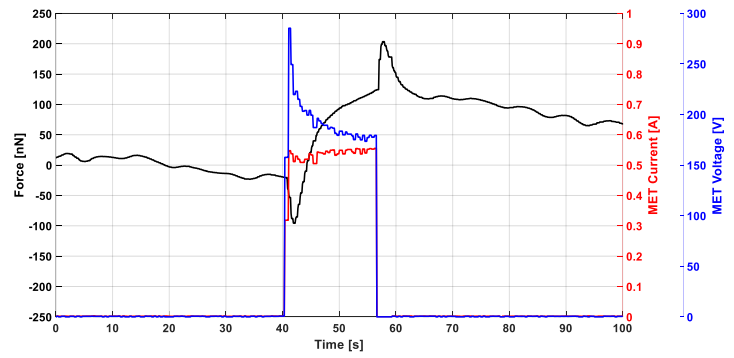


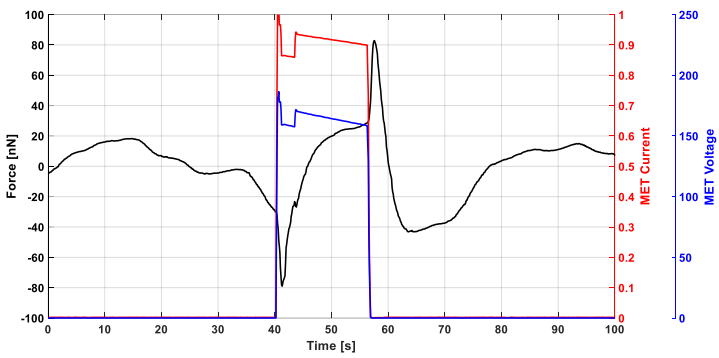
Figure 20: Fixed frequency, 36.0 kHz, 16 s pulse with NS5, Fullerton electronics, and copper block



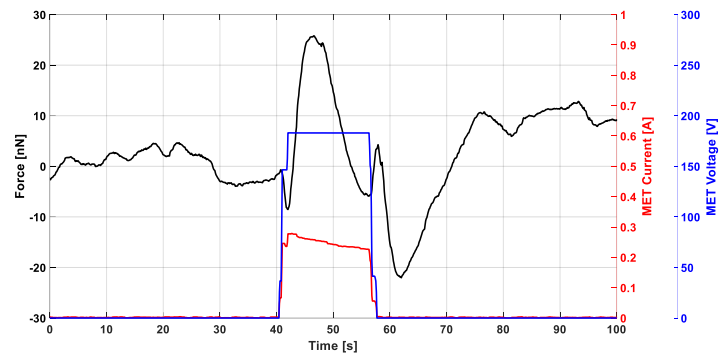
a) Fullerton electronics, 36.0 kHz, without copper block



b) Fullerton electronics, 36.3 kHz, with vibration-isolation yoke



c) Fullerton electronics, 30.0 kHz, with copper block



d) Dresden electronics, 36.0 kHz, with copper block

Figure 21: Fixed frequency, 16 s pulse with NS5 180° orientation

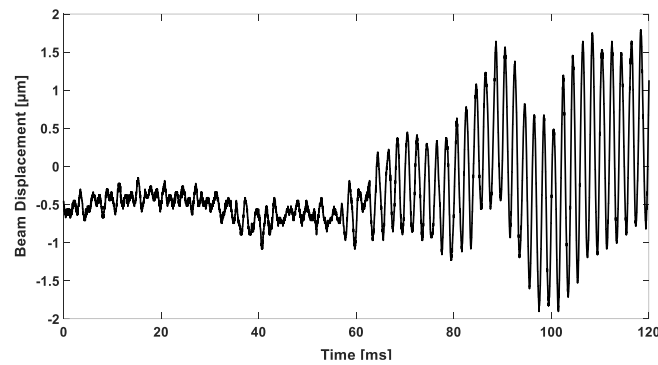


Figure 22: Beam vibration analysis of NS5 with Fullerton electronics (-90° orientation)